Development of x-ray scintillator functioning also as an analyser grating used in grating-based x-ray differential phase contrast imaging*

Lei Yao-Hu(雷耀虎), Liu Xin(刘 鑫), Guo Jin-Chuan(郭金川), Zhao Zhi-Gang(赵志刚), and Niu Han-Ben(牛憨笨)†

Key Laboratory of Optoelectronics Devices and Systems of Ministry of Education, Institute of Optoelectronics, Shenzhen University, Shenzhen 518060, *China*

(Received 11 August 2010; revised manuscript received 9 October 2010)

In order to push the grating-based phase contrast imaging system to be used in hospital and laboratories, this paper designs and develops a novel structure of x-ray scintillator functioning also as an analyser grating, which has been proposed for grating-based x-ray differential phase contrast imaging. According to this design, the scintillator should have a periodical structure in one dimension with the pitch equaling the period of self-image of the phase grating at the Talbot distance, where one half of the pitch is pixellated and is made of x-ray sensitive fluorescent material, such as CsI(Tl), and the remaining part of the pitch is made of x-ray insensitive material, such as silicon. To realize the design, a deep pore array with a high aspect ratio and specially designed grating pattern are successfully manufactured on 5 inch silicon wafer by the photo-assisted electrochemical etching method. The related other problems, such as oxidation-caused geometrical distortion, the filling of CsI(Tl) into deep pores and the removal of inside bubbles, have been overcome. Its pixel size, depth and grating pitch are 3 μm×7.5 μm, 150 μm and 3 μm, respectively. The microstructure of the scintillator has been examined microscopically and macroscopically by scanning electron microscope and x-ray resolution chart testing, respectively. The preliminary measurements have shown that the proposed scintillator, also functioning as an analyser grating, has been successfully designed and developed.

Keywords: scintillator screen, pore arrays, oxidation, CsI(Tl), analyser grating

PACS: 29.40.Mc, 07.85.Fv, 87.57.Cf **DOI:** 10.1088/1674-1056/20/4/042901

1. Introduction

Images of biological soft tissues and their formed organs inside the body, polymers or fibre composites consisting of low-Z elements, which cannot be obtained by conventional x-ray absorption imaging with high image contrast, can be successfully provided by a novel technique of x-ray phase contrast imaging based on a synchrotron radiation x-ray source.[1−3] Some schemes of x-ray phase contrast imaging based on table-top x-ray sources have been proposed and developed since the proposition of the technique of in-line phase contrast imaging by Wilkins *et al.* In 1996,[4,5] showed the potential of applications in clinical and industrial fields. Among them, the grating-based differential phase contrast imaging developed by Pfeiffer *et al.* in 2006 is more attractive due to its uncritical requirements on coherent characteristics of an x-ray source.[6] Although the enormous advantages have been proven for the above phase contrast imaging over conventional absorption technique, its application is still very limited by the lack of powerful table-top x-ray source and techniques for making widely used x-ray devices, such as phase grating, analyser grating and x-ray digital detector with large enough effective working size. Recently, some efforts have been made on the development of an x-ray source with high power and partially spatial coherence,[7−9] and qualified phase gratings with big enough effective size produced by us and others with an existing manufacturing technology.[10] However, the analyser grating is very costly and its size is very limited, while either the size or the spatial resolution for the x-ray detector is also very limited, therefore they cannot easily be used in hospitals. Hence, a novel idea of an x-ray scintillator functioning also as an analyser grating was proposed by us for the grating-based x-ray differential phase contrast imaging.[11] According to this idea, a novel structure of x-ray scintillator has been designed and developed. Based on our design, the scintillator

*Project supported by the Major Program of the National Natural Science Foundation of China (Grant No. 60532090).

†Corresponding author. E-mail: hbniu@szu.edu.cn

© 2011 Chinese Physical Society and IOP Publishing Ltd

should have a periodical structure in one dimension with the pitch equaling the period of self-image of the phase grating at the Talbot distance, where one half of the pitch is pixellated and is made of x-ray sensitive fluorescent material, such as CsI(Tl), and the remaining part of the pitch is made of x-ray insensitive material, such as silicon. The x-ray can be converted into visible light by deep pore arrays filled with fluorescence material CsI(Tl), which occupies a half period of the grating, and for the remaining part of the grating made of full silicon, where there is not any visible light generated by the input x-ray to make a visible light detector, such as a coupled charge device (CCD), detectable, which functions as a scintillator and also an analyser grating. According to the principle of the x-ray Talbot interferometer, combined with the phase grating, the above x-ray scintillator coupled with a CCD detector through a fibre plate or a fibre tape can detect a differential phase shift caused by an object placed normally in front of the phase grating.[6] The difference between our scheme and the usual one is that the hard x-ray is passing through the silicon grating almost completely in our case other than absorbed by a high Z element such as a Au filled analyser grating as usual, but their functions are the same, making the x-ray within a half period of the analyser grating undetectable. Furthermore, the x-ray scintillator functioning also as an analyser grating, which is fabricated by our developed methods and experimental setup, is more beneficial for simplification of the imaging system and improvement of image contrast than the one combining the thin analyser grating with the usual x-ray detector. In addition, the low cost of the analyser grating with our method also promotes phase-contrast imaging that is applicable to common laboratories and hospitals. The issue is whether we can develop this kind of scintillator from the existing technology. Therefore, this paper will outline the main points of its design and fabrication, from which one can know how this device can meet the characteristic requirements of the grating-based differential phase contrast imaging. Under consideration of playing the role of an analyser grating, the scintillator should possess a small enough pitch and naturally provide very high spatial resolution. The main difficulty is how its sensitivity to hard x-rays can be improved and at the same time its structure can meet the requirements of the analyser grating.

2. Design of scintillator

The complex transmission function $T(x)$ of the phase grating can be expressed with the Fourier series as

$$T(x) = \sum_{n=-\infty}^{\infty} a_n \exp\left(\mathrm{i}\, n \frac{2\pi}{p_1} x\right), \tag{1}$$

where a_n is the amplitude of the n-th harmonic and p_1 is the period of the grating. For the case of using a one-dimensional spatial coherent x-ray source, only one-dimensional expressions are given. The complex amplitude of the propagating field at a distance l behind the phase grating illuminated by a plane wave is given by

$$U(x,z) = \sum_n a_n \exp\left(-\mathrm{i}\,\pi n^2 \frac{l\lambda}{p_1^2}\right) \exp\left(\mathrm{i}\, n \frac{2\pi}{p_1} x\right). \tag{2}$$

The self-image will be observed at the Talbot distance, when an object is placed before the phase grating. Considering the optimum diffraction efficiency, we can write the intensity of the image at the Talbot distance as

$$I_{\mathrm{c}}(x) = \frac{8}{\pi^2} A^2(x) \left[1 + \cos\frac{2\pi}{p_2}\left(x - l\frac{\lambda}{2\pi}\frac{\partial\varphi}{\partial x}\right)\right], \tag{3}$$

where φ and A are the phase-shift and absorption component of the object, respectively, and p_2 is the period of the fringes. In order to transform the phase modulation of fringes into an intensity modulation, an analyser grating is usually placed immediately before the traditional x-ray scintillator. If the analyser grating is integrated into the scintillator, the new scintillator will have dual functions of the common detector and the analyser grating. According to the idea mentioned above, the structure and detecting principle of the new scintillator is illustrated below. On the assumption that the period of the scintillator coincides with the period of the fringes p_2, and that the width of the sensitive part of the scintillator to hard x-ray in one period is D and the width of the visible light pixel of CCD is L, as shown in Fig. 1,[11], the intensity in one period of fringes is

$$I' = \kappa \int_{\chi}^{\chi+D} I(x)\mathrm{d}x, \tag{4}$$

where κ is the transforming efficiency of the scintillator and χ is the displacement of the interference fringes with respect to the scintillator screen. When one visible light pixel of the CCD collects N periods of fringes, the intensity signal of one pixel is

$$I_{\mathrm{m}} = \kappa\Big[\int_{\chi}^{\chi+D} I(x)\mathrm{d}x + \int_{p_2+\chi}^{p_2+\chi+D} I(x)\mathrm{d}x + \cdots$$

$$+\int_{(N-1)p_2+\chi}^{(N-1)p_2+\chi+D} I(x)\mathrm{d}x\Bigg] = NI'. \quad (5)$$

To improve the spatial resolution of the whole imaging system, N should be equal to or less than the periodical number of the x-ray source. Considering Eq. (3), we rewrite Eq. (5) as

$$I_{\mathrm{m}} = \kappa N A_{\mathrm{m}}^2 p_2 * \left\{\gamma + \frac{1}{\pi}\cos\left[\gamma\pi - z\frac{\lambda}{p_2}\frac{\partial\varphi}{\partial x} + \frac{2\pi\chi}{p_2}\right]\sin(\gamma\pi)\right\}, \quad (6)$$

where $2\pi\chi/p_2$ is the initial phase of fringes, and γ ($\gamma = D/p_2$) is the aspect ratio of the scintillator. Obviously, the optimal value of γ is 1/2 for the modulation of phase information $\sin(\gamma\pi)$ has the maximum value, which means that the optimum structure of the scintillator is that one half of the period is sensitive to the x-ray and the remaining part of the period is not.

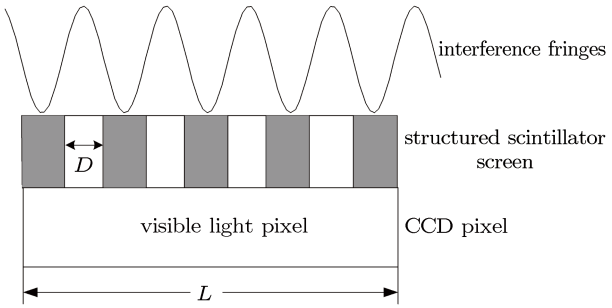


Fig. 1. The model of detecting interferogram with a structured x-ray scintillator screen.

From the above analyses, we can conclude that the scintillator also functioning as an analyser grating should have a periodical structure in one dimension with the pitch equaling the period of self-image of the phase grating at the Talbot distance, where one half of the pitch is pixellated and is made of x-ray sensitive fluorescent material, such as CsI(Tl), and the remaining part of the pitch is made of x-ray insensitive material, such as silicon.

3. Fabrication of scintillator

3.1. Fabrication of deep pore arrays

In order to meet the structural requirements of the scintillator and analyser grating simultaneously, as stated above, our scintillator exhibits a periodical structure in one dimension, one half of the period is sensitive to x-ray and the remaining part of the period is not. In another dimension, the part sensitive to x-rays is divided into pixels. It is essential for our scheme to fabricate the fundamental configuration with silicon wafer by mature technology. We employed and developed the photo-assisted electrochemical etching technique to fabricate the high aspect ratio pore arrays in 5-inch n-type (1 0 0) silicon wafer. The process can be divided into two main steps. The first step is to generate pits, where the pores are supposed to be extended, by KOH solution with a concentration of 10%. The second step is to generate pores along the pits by a photo-assisted electrochemical etching method, initially invented by Lehmann *et al.* and developed by us.[12,13]

As is well known, regular pore arrays were generated according to the Lehmann formula,

$$J_{\mathrm{ps}} = Cc^{1.5}\exp\left(-E_{\mathrm{a}}/(K_{\mathrm{B}}T)\right), \quad (7)$$

where J_{ps} (in A·cm^{-2}) is the current density mainly determined by the concentration of HF, denoted by c in weight ratio, and its temperature, $C = 3300$ A/cm^2 and $E_{\mathrm{a}} = 0.345$ eV.[14]

Unfortunately, when we made our device under guidance of this equation, the appearance of the etched wafer was quite different from our designed configuration. From our analysis, the reason originates from the life time and diffusion coefficient of minor carriers in the n-type silicon. When the thickness of the silicon wafer is greater than 300 μm (400 μm in our case), most of the minor carriers generated by the back-illuminated light cannot reach the chemical reaction pit locations due to their too short life time of about 10 μs. In order to etch the pits at the reaction surface attached with HF acid, the near infra-red light with a wave length of 900 nm–1100 nm generated by tungsten–halogen lamps has to be used to generate minor carriers directly near the reaction surface due to their small absorption coefficient in silicon wafer.[15] But at the same time, this measure will bring about a side effect, directly conducting side etching due to the local generation of minor carriers in the space charge region, therefore the current to the pits and side wall will be redistributed and the etched pattern becomes an unwanted manner. To solve this problem, we have taken two measures. Firstly, the voltage applied to the silicon wafer has been enhanced to collect more minor carriers to the pits generated not only in the field free region but also in the space charge region to meet the requirement on the pit etching current and also to reduce the side etching effects. The second but more important measure taken by us is of modification of the current density defined by the Lehmann formula:

$$J_{\mathrm{ps}} = Cc^{1.5}\exp\left(-E_{\mathrm{a}}/(K_{\mathrm{B}}T)\right)\left(1+\alpha t+\beta t^2\right), \quad (8)$$

where t is etching time in minutes, and α and β are two constants for the modification of etching current density. According to our etching process, a rectangular pore array was fabricated according to Eq. (8) in 5-inch (1 0 0) silicon wafer, where each pore has a wall width of 600 nm and consists of four sub-pores whose wall width is 250 nm in one dimension and the common wall width for all pores is 1.5 μm in another dimension. As a scintillator, its pixel size formed by 4 sub-pores is 3 μm×7.5 μm and each sub-pore size is about 3 μm×1.9 μm, where cross-talk among sub-pores in the same pixel may occur due to a thin wall between them. As an analyser grating, the pitch is 3 μm and the width of the silicon wall is 1.5 μm. The reason for the design of the sub-pore structure is to make the etching feasible. Of course, we can make the pixel size as small as the sub-pore or even smaller, but the sensitivity of the scintillator will become lower due to too little fluorescent material of CsI(Tl) to be filled. It should be mentioned here that among the above dimensional figures, the silicon wall width of 1.5 μm is essential to the grating of the analyser. The deviation from the wall width of 1.5 μm depends on the depth of the sub-pores, which defines the sensitivity of the scintillator to the x-ray. According to our present technique, this wall thickness is between 0.9 μm–1.5 μm from the top to the bottom of the sub-pores if their depth is 150 μm. From our numerical simulation, the obtained dimensional figures as stated above are admitted for a qualified analyser grating, which will be reported elsewhere. A photograph of a scanning electron microscope (SEM) is shown in Fig. 2, where figure (a) gives the local structure, none of the vanished pores can be observed, while figures (b) and (c) show the whole structure observed in the different directions, respectively. Figure (b) displays clearly its structure as an analyser grating and figure (c) shows its manner as a configuration of the scintillator.

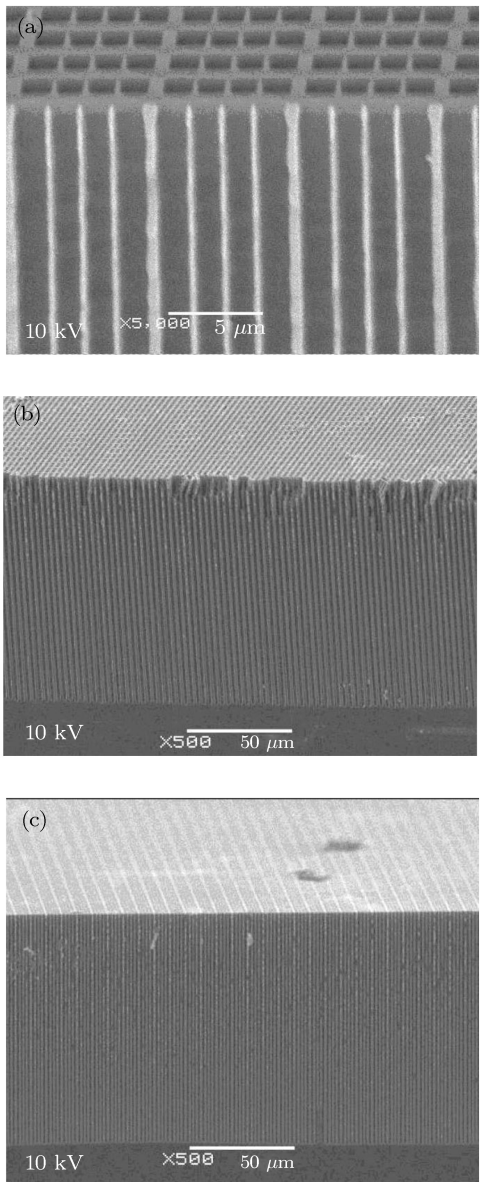


Fig. 2. A novel pattern of pore arrays used as a fundamental configuration of the scintillator and also the grating of the analyser: (a) part of the local structure; (b) the structure as an analyser grating observed in one direction; (c) the structure as a configuration of the scintillator observed in the direction perpendicular to (b).

3.2. Oxidation and filling with CsI(Tl)

The silicon pore arrays are oxidized in order to obtain an array of scintillating waveguides, whose operation principle is similar to the scintillating optical fibre. As is well known, the index of refraction of silicon is about 3.4, which is much larger than that of the scintillating material CsI(Tl) of about 1.78. In order to reduce the index of refraction of the silicon wafer locally, the wall surface of the sub-pores needs to be oxidized. To obtain a more compact oxidation layer on the sub-pore wall surface, the procedure of dry thermal oxidation is preferable to the wet one. After the silicon wafer with perfect pore arrays is kept in the oxidation furnace under the condition of O_2 at 1100 ° for 1 hour, then the SiO_2 layer with a thickness of about 250 nm on the wall surface of sub-pores can be generated. Unfortunately, no matter which oxidation approach is taken, wet or dry thermal oxidation, the deformation of silicon wafer is always inevitable, especially for our large size. For a flat silicon wafer with a diameter of 5 inches, the deformation in its thickness dimension can even reach as much as 4 mm after

oxidation. Obviously, it cannot be directly filled with CsI(Tl) and coupled with the CCD detector through a fibre tape or a fibre plate. An approach of rectification of the oxidized silicon wafer with a specially designed adjustable ring mounting support, which has turned out to be an effective method and results in a satisfying surface, has been proposed and developed, as shown in Fig. 3.



Fig. 3. After rectification of the oxidized silicon wafer with an adjustable ring mounting support.

Filling pore arrays with CsI(Tl) is the last but key procedure for the fabrication of the scintillator. This work has been done by several groups, but either the pore size is rather large or the depth of the pore array is small.[16−18] Compared with others, the size and depth of our sub-pores are about 1.5 μm×1.9 μm and 150 μm, respectively, which is much more difficult for CsI(Tl) to be filled. The main point of our procedure is how we can exploit the vacuum characteristics of narrow and deep sub-pores to be filled with CsI(Tl) without bubbles anywhere inside the sub-pores and make the surface of the silicon wafer CsI(Tl)-free. To this end, we have developed a filling setup and a complete procedure. What we should emphasize here is the fact that the sub-pores are evacuated thoroughly at the beginning for a bit longer time, CsI(Tl) powder over the surface of the silicon wafer is then heated up to its melting temperature within a short period of time, and at the same time the chamber, where the silicon wafer is mounted, is filled with nitrogen to about 1 atmosphere pressure, and finally the chamber is evacuated again and the remaining CsI(Tl) on the surface of the wafer clears up by sublimation. The filling result is given by SEM photograph in Fig. 4.

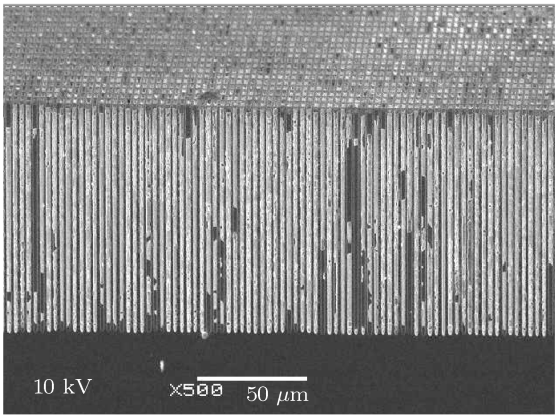


Fig. 4. The result of filling with CsI(Tl) in the sub-pores by our developed techniques.

4. Further examination of the scintillator

The micro-structures of our scintillator have been measured by SEM from different fields of view with different parts of the scintillator. However, we cannot conclude from the SEM sampled examination that the scintillator is qualified because only very limited parts of the sample were evaluated. We need to check its microstructures and performances from a macroscopic point of view. The ultimate evaluation of the scintillator will be performed by phase contrast imaging, which is prepared in our laboratory. There are many different fine and fixed structures on the x-ray resolution chart. Therefore the spatial resolution chart testing for the scintillator not only provides its spatial resolving power but also implies information about its microstructures from a macroscopic point of view. For doing so, the different part of the scintillator is coupled directly to a CCD with pixel size and pixel number of 13.5 μm×13.5 μm and 2048×2048, respectively, through a fibre plate from time to time. During testing, the x-ray source equipped with a structured-anode x-ray tube developed by us is used. The voltage applied to the x-ray tube is 60 kV. In order to check the whole scintillator, we moved the x-ray resolution chart everywhere on it and one of the results is shown in Fig. 5. The maximum resolution of our x-ray resolution chart is 20 lp/mm, which can be clearly discerned on the output image. From Fig. 5, we can also find that there are no blemishes generated by the defects of the scintillator microstructure on the image of the x-ray resolution chart. Some black and white spots can be seen in Fig. 5. They do not attribute to the defects

of its microstructure, but the black spots are caused by the dust over the surface of the silicon wafer, which prevents the x-ray induced visible light from reaching the CCD detector and the white spots are generated due to the stochastic noise of the CCD.

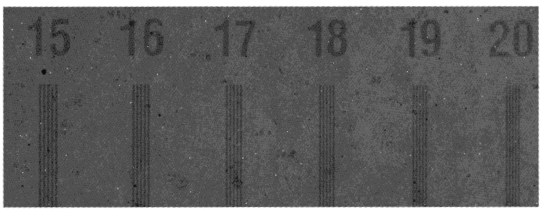


Fig. 5. Resolution testing of the scintillator with x-ray resolution chart.

5. Conclusion

Design and fabrication of a novel x-ray scintillator functioning also as an analyser grating have been achieved according to our scheme for the grating-based x-ray differential phase contrast imaging. Though the processes of fabrication, including fabrication and oxidation of deep pore arrays and filling with fluorescent material CsI(Tl), are complicated and indeed challenging, a series of problems have been solved and a qualified scintillator has been made with our developed technology, which has been preliminarily manifested by SEM measurements and resolution chart testing.

Acknowledgements

We would like to acknowledge Shenzhen Si Semiconductors CO, LTD for providing high-quality silicon wafers and also thank Ms. Gui-Wen Xu for her microscopy testing of pore arrays and scintillators.

References

[1] Momose A, Takeda T, Itai Y and Hirano K 1996 *Nature Med.* **2** 473

[2] Chapman D, Thomlinson W, Johnston R E, Washburn D, Pisano E, Gmur N, Zhong Z, Menk R, Arfelli F and Sayers D 1997 *Phys. Med. Biol.* **42** 2015

[3] Snigirev A, Snigireva I, Kohn V, Kuznetsov S and Schelokov I 1995 *Rev. Sci. Instrum.* **66** 5486

[4] Wilkins S W, Gureyev T E, Gao D, Pogany A and Stevenson A W 1996 *Nature* **384** 335

[5] Nugent K A, Gureyev T E, Cookson D F, Paganin D and Barnea Z 1996 *Phys. Rev. Lett.* **77** (14) 2961

[6] Pfeiffer F, Weitkamp T, Bunk O and David C 2006 *Nature Phys.* **2** 258

[7] Niu H B, Guo J C, Wang K G and Yang Q L *PRC Patent* 200610062487.1 [2006-10-06] (in Chinese)

[8] Momose A, Wataru Y, Hiroaki K and Katsuyuki K 2009 *Jpn. J. Appl. Phys.* **48** 076512-1

[9] Olivo A, Bohndiek S E, Griffiths J A, Konstantinidis A and Speller R D 2009 *Appl. Phys. Lett.* **94** 044108-1

[10] Liu X, Lei Y H, Zhao Z G, Guo J C and Niu H B 2010 *Acta Phys. Sin.* **59** 6927 (in Chinese)

[11] Liu X, Guo J C and Niu H B 2010 *Chin. Phys.* B **19** 070701

[12] Lehmann V and Föll H 1990 *J. Electrochem. Soc.* **137** 653

[13] Lei Y H, Guo J C, Zhao Z G and Niu H B 2010 *Semiconductor Technology* **35** 517 (in Chinese)

[14] Lehmann V 1993 *J. Electrochem. Soc.* **140** 2836

[15] Lehmann V 2002 *Electrochemistry of Silicon* (Weinheim: Wiley-VCH) pp. 133–138

[16] Olsen U L, Schmidt S, Poulsen H F, Linnros J, Yun S H, Michiel M Di and Martin T 2009 *Nucl. Instr. Method* A **607** 141

[17] Badel X, Linnros J, Janson M S and Österman J 2003 *Nucl. Instr. Method* A **509** 96

[18] Simona M, Engel K, Menser B, Badel X and Linnros J 2008 *Nucl. Instr. Method* A **591** 291